



Bachelor thesis

Sidsel Borup Winther

Exploration of Atomic Force Microscopy and Domain Formation in Supported Lipid Bilayers

Supervisors: Thomas Heimburg and Rima Budvytyte

Date: 15 June 2016

Abstract

Nerve signal propagation is one of the most prominent aspects of signaling processes in biological membranes. Based on the observation of phase transition phenomena during the propagation of nerve signals, it is suggested that the domain formation in phase transitions of lipid membranes associated with hydrophobic mismatch will influence the signal propagation.

With mica-supported DPPC bilayers as model system, atomic force microscopy was utilized to study the domain formation through the main phase transition. In accordance with the influence of mica-support on phase transitions in DPFC double bilayers obtained from differential scanning calorimetry by Yang and Appleyard, a splitting of the phase transition was found. Three types of distinguishable domain formation were observed, suggesting a variation in both the inter and intra leaflet interactions within bilayers.

The height changes associated with phase transition was found to correspond to a 65% change in the membrane capacitance, indicating a non-negligible change in the membrane capacitance during the propagation of a nerve signal as it is otherwise assumed the Hodgkin-Huxley Model for propagation of nerve signals.

Acknowledgements

I especially want to thank Thomas Heimburg and Rima Budvytyte. Thomas, for making this project possible and for providing essential feedback, that has formed this project. Rima, for guidance in the introduction to working with the atomic force microscopy throughout the project work.

Table of contents

1	Introduction	2
2	Theoretical background	3
2.1	Structure of lipid bilayers	3
2.2	Configurations of lipids and phase separation	4
3	Experimental approach	5
3.1	Preparation of supported lipid bilayers	5
3.2	Topographic measurements with atomic force microscopy	6
3.2.1	The ground principle	6
3.2.2	Instrumental setup for atomic force microscopy	7
3.2.3	Important parameters	8
3.3	Processing of raw data	9
3.4	List of materials	9
3.5	Results	10
3.5.1	First results	10
3.5.2	Scanning of mica	11
3.5.3	The influence of media and setpoint on scanings of a calibration grid	11
3.5.4	The effect of cantilever spring constant on SLBs	12
3.5.5	The effect of setpoint on SLBs	13
3.5.6	Temperature induced phase transition in DPPC SLB	14
4	Discussion and conclusions	17
4.1	Disclosure of experimental limitations	17
4.2	Temperature induced phase transitions in a mica-supported DPPC bilayer	17
4.3	Further explorations	18
5	References	20
A	Appendix	21
A.1	Increased sensitivity due to refraction index	21
A.2	AFM probe: PNP-TR-20 purchased from NanoWorld	22
A.3	AFM probe: ACTA purchased from AppNano	23
A.4	Drift in position for each scanning	24

1 Introduction

Every biological cell is confined by a semipermeable membrane with the main purpose of separating the inner and outer environment. This separation gives rise to gradients across the membrane, that drive several inter and intra cellular processes.

In 1972 Singer and Nicolson proposed the Fluid Mosaic model to describe the structure of cell membranes [1]. The model describes the structure of the membrane as a two-dimensional oriented viscous solution with lateral mobility. The solution is constituted by a bilayer of lipids, wherein proteins are embedded - mainly due to hydrophobic interactions. The lateral organization of lipids is suggested to exhibit short-range order caused by the interaction between lipids and proteins. This short-range order gives rise to the formation of domains. The principle from the Fluid Mosaic Model was in 1984 expanded by Mouritsen and Bloom in the Mattress model [2]. In this model the short-range order is assigned to hydrophobic mismatch due to different lengths of the hydrophobic regions of proteins and lipids. Since biological membranes contain hundreds of different lipid species with different head groups and chain composition, similar arguments lead to the assumption, that also the lateral organization of different lipid species is influenced by hydrophobic mismatch.

In both models the membrane is described as a dynamic structure. It is evident that the dynamic structure is crucial for the functioning of cells [3]. The dynamic organization of the membrane makes it sensitive to perturbations of the system by e.g. temperature, pressure and drugs, making the membrane an ideal vehicle for signaling processes. One of the most prominent aspects of signaling processes for cells is the propagation of nerve signals. This process enables life in the complex multicellular form that we know from animals where the needed interaction with the world is made possible by exactly propagation of nerve signals.

Different models have been proposed for the propagation of nerve signals. The currently most commonly accepted model was proposed by Hodgkin and Huxley in 1952 [4]. The model is based on equilibration of several trans-membrane ionic gradients through specific ion-conducting proteins, which results in a transient voltage change across the membrane. In the picture of the model the ion-conducting proteins are homogeneously distributed along the membrane of the axon of the nerve. When the ion-conduction proteins locally open due to the voltage change, it influences the electric potential in their environment, and leads to opening of nearby channels as well. This makes the voltage change propagate down the axon of the nerve cell. The propagation is described by the following differential equation

$$K \frac{\partial U(x, t)^2}{\partial x^2} = C_m \frac{\partial U(x, t)}{\partial t} + \sum_i g_i (U(x, t) - E_i), \quad (1)$$

where K is a constant depending on the specific properties of the nerve, $U(x, t)$ is the voltage, x is the direction along the axon, t is time, C_m is the capacitance of the membrane, g_i is the resistance of the i 'th type of ion-conducting protein. In this representation, the propagation of the nerve signal is modeled as being dissipative. Hence, the process must generate heat. However, experimental results do not show a net production of heat. This suggests that the process is instead adiabatic [7].

In 2005 Heimburg and Jackson proposed The Soliton Model where nerve signals are treated as propagating density pulses in the nerve axon membrane [5]. The density pulses have properties of solitons, i.e. they propagate without attenuation and without changes in shape. The existence of solitons require nonlinear elastic constants upon density changes of the media, and dispersion, i.e. frequency dependence of sound velocity. Both conditions are met in the membranes of nerve cells. Biological membranes display a melting transition just below body temperature. Therefore only slight changes are necessary to induce a phase transition in the membrane of the nerve cell, and it can be done by increasing the lateral pressure of the membrane. During the phase transition the heat capacity, volume compressibility, area compressibility, and relaxation times all reach a maximum. Hence, the elastic constants are nonlinear upon density changes. Furthermore it has experimentally been found that membranes display dispersion.

The propagation of the nerve pulse is described by

$$v^2 \frac{\partial^2}{\partial z^2} \Delta \rho^A = \frac{\partial}{\partial z} \left(c^2 \frac{\partial}{\partial z} \Delta \rho^A \right) - h \frac{\partial^4}{\partial z^4} \Delta \rho^A, \quad (2)$$

where v is the propagation velocity, z is $x - vt$, $\Delta\rho^A$ is the change in lateral density, c is the velocity of sound given by $\sqrt{(\rho_0^A k_s^A)^{-1}}$ with k_s^A being the lateral compressibility, and h is a dispersion parameter.

The Soliton Model explains several experimentally found properties of nerve signal propagation, which are not included in the Hodgkin-Huxley Model. Examples are changes in the thickness of the membrane, changes in the length of the nerve, reversible heat production, nerve propagation triggered by cooling [6] and the existence of phase transition phenomena.

However, common for the two models are, that properties of the membrane influences the propagation of the nerve signal. The Hodgkin-Huxley model depends on (but not only) the permeability and capacitance of the membrane, and the Soliton model depends on (but not only) the compressibility of the membrane. Hence, a change in these parameters will influence the propagation of a nerve signal.

As mentioned above, biological membranes display a melting transition just below body temperature, and it has been found, that nerve signals can be induced from cooling [6]. During a phase transition there will, due to changes in the lipid composition, occur a phase separation to decrease hydrophobic mismatch. The phase separation phenomena will therefore lead to the formation of domains. At the domain interfaces fluctuations are at the maximum, therefore also elasticity and compressibility are. Due to hydrophobic mismatch also the permeability is increased. This suggests that the formation of domains is relevant to study regarding to propagation of nerve signals.

To study the formation of domains it is necessary to isolate the phenomena from the various other phenomena that occur in the complex multicomponent biological membrane. For this purpose a simplified model system, consisting only of lipids (referred to as lipid bilayers), is introduced.

2 Theoretical background

To understand the formation of domains in lipid bilayers it is necessary to understand the structuring of these bilayers and the change in configuration of lipids that causes a phase transition of the lipid bilayer. Domains form due to hydrophobic mismatch which among other is a consequence of the height change associated with the phase transition.

2.1 Structure of lipid bilayers

Lipids are amphiphilic molecules, i.e. they possess both hydrophilic (water loving, polar) and hydrophobic (water hating, non-polar) properties. There exists a large variety of lipids, but the type that is most essential for the lipid bilayer of biological membranes are phospholipids, since these are the lipids that make up the structural part of the membranes. Phospholipids are composed of a hydrophilic phosphate head and a number of hydrophobic hydrocarbon chains (see Figure 1, left). The phospholipids differ from each other mainly by differences in number, length and saturation of the hydrocarbon chains, and by head group.

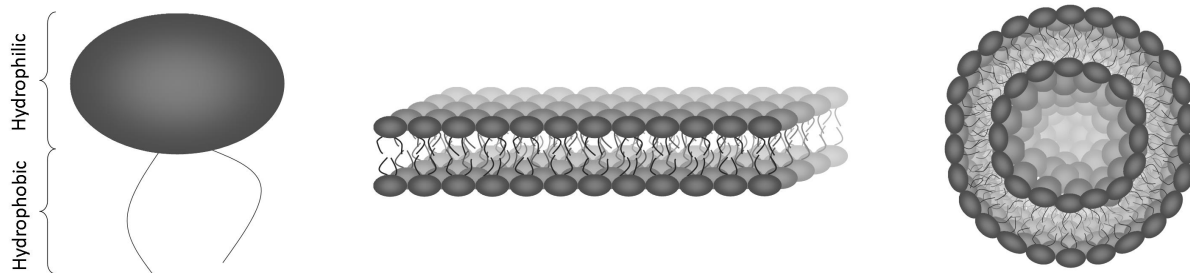


Figure 1: Schematic illustration of self-assembled lipid structures. Left: A lipid illustrating a hydrophilic head and two hydrophobic hydrocarbon chains. Center: Lipids self-assembled to form a bilayer. Right: Cross section of lipids self-assembled to form a vesicle.

Because of the repelling hydrophobic interactions between water and the hydrocarbon chains, the free energy state is decreased when such interactions are avoided. Therefore, when the lipids are exposed to

water they will self-assemble into structures that are decreasing the energy of the system by isolating the hydrophobic ends from the water. These structures are also found to increase the entropy of the system. The structures are supra-molecular, meaning that the lipid molecules are held together by non-covalent bonds and hence not sharing electrons. The dominating interactions between the lipids are electrostatic. Most relevant for modeling biological membranes is the planar bilayer structure (see Figure 1, center) and the vesicle structure (see Figure 1, right), which is a spherical formation of the bilayer. Both structures can appear multilamellar. The thickness of the bilayer depends on the length of the hydrocarbon chains of the lipids.

The bilayer is organized as a liquid-crystalline, i.e. an intermediate phase between liquid and crystalline, with both positional and orientational order. The bilayer structure is well-defined, but dependent on the phase, the lipids are able to flow within the bilayer.

2.2 Configurations of lipids and phase separation

Several conformations are possible for the hydrocarbon chains of the lipids. The different conformations are generated by rotation around the bonds between the carbons (known as trans-gauche isomerizations) and depend on the energy of the system. The lowest energy conformation appears when all bonds are in the trans configuration. In this configuration the hydrocarbon chains will appear completely ordered and extended to the maximum. By increasing the energy of the system, gauche-isomers will be induced. This results in higher degeneracy (and entropy) and the hydrocarbon chains will instead appear disordered and less extended. Thus, the configuration of the lipids is temperature dependent.

The assembly of many interacting lipids obtains properties that no lipid possesses by itself. This leads to a cooperative interaction with regards to the configuration of the individual lipid, and causes transitions between different states of the lipid bilayer at well defined temperatures. For an increasing amount of molecules, the phase transition becomes more distinct.

The configuration of the lipids effect the organization of the bilayer. For signal propagation in lipid membranes, the two most prominent configurations are the *gel phase* and the *fluid phase*. In the gel phase the hydrocarbon chains are ordered. This enables a closer packing of the lipids and leads to stronger electrostatic forces between the head groups, causing the lateral order of lipids to be crystalline. In the fluid phase the hydrocarbon chains are disordered. This leads to weaker electrostatic forces between the head groups and enables a higher degree of diffusion of lipids with the bilayer, causing the lateral order of lipids to be random. The two configurations are schematically illustrated in Figure 2. A distinct change in bilayer thickness can be measured when the lipids are taken through their main phase transition.

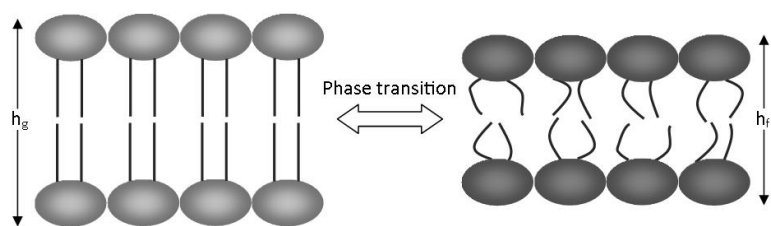


Figure 2: Schematic illustration of the transition between the gel and fluid phase. During the transition the enthalpi and entropi of the lipids changes, which links the melting transition to a loss of order in the chains. Hence the thickness of the membrane decreases. h_g and h_f indicates the height of the gel phase and fluid phase respectively.

The transition between the configuration of a lipid occurs in fluctuations. Hence, even for a single component lipid bilayer, not all lipids go through the transition at the exact same time. Due to the change in height associated with the transition this leads to hydrophobic mismatch between unlike lipids and increased interfacial energy (also known as line tension). To minimize the increase of free energy caused by the hydrophobic mismatch, the two phases will separate to decrease the interface between them. This leads to the formation of domains. A schematic illustration of a gel phase domain forming in the fluid phase is seen in Figure 3.

The interfacial energy between unlike lipids is an essential parameter for determining how the domains form. When fluid domains form in a fluid environment (could be for a two-component membrane), they

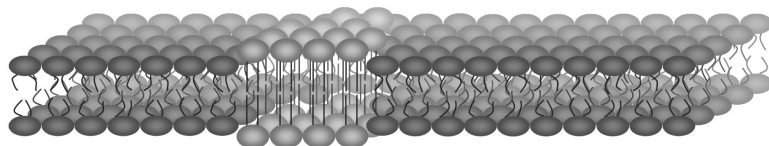


Figure 3: Schematic illustration of a gel phase domain formed in a fluid phase.

will initially appear circular because both parts allow for diffusion and the perimeter is minimized by optimizing the area-to-perimeter ratio [11]. When the domain formation occurs in a different phase the shape of the domains will initially be more restricted. Very complex shapes can arise from the competition between line tension and the electrostatic interaction between different parts in the membrane. Hence, for one-component membranes the most restricted domain formation will appear in the gel-fluid transition, and a less restricted domain formation will appear in the fluid-gel transition. When the system is equilibrated, the shape of all types of domains will be rounded.

3 Experimental approach

The change in the height of the lipids associated with the phase transition for lipids can be utilized to determine the lateral structure of lipid bilayers by measuring the topographic properties. The topographic properties can be measured using atomic force microscopy (AFM). This method is based on the measurements of the interactions between a mechanical tip and a sample (the tip-sample interactions), while the tip is scanned across the sample (or opposite). The method was implemented experimentally for the first time by Binnig, Quate and Gerber in 1985 [12]. By combining AFM and fluorescent microscopy it has been confirmed that height differences measured with AFM correspond to different phases [21].

As with any model system it is essential to adapt the system to provide the relevant information. Therefore the lipid bilayers were created from lipids with identical head groups that only deviates in the length of the hydrocarbon chains. Since the curvature of a reasonable vesicle would be much larger than the scale of the lateral structure of interest, it is an advantage to do the measurements on a planar area. Also therefore, lipid bilayers on planar hydrophilic supports are used. In this way the three dimensional structure of a spherical vesicle is simplified to two dimensions. From comparing results obtained by fluorescence microscopy and by AFM it has been found that the fraction of domains in giant unilamellar vesicles (GUVs) and in planar bilayers are similar [11]. This indicates that a system of supported lipid bilayers can provide the desired information about domain formation. For this project only mica has been used for support. Mica is a crystalline structure with a hexagonal sheet-like arrangement of its atoms that gives it a nearly perfect cleavage. Thus the use of freshly cleaved mica ensures a clean and flat support for the lipid bilayer. However, the presence of a support has been shown to have an effect on the symmetry between the two leaflets of a bilayer, since a coupling between the lower leaflet and the support occurs [25]. This might cause decoupling of the two leaflets of a bilayer that is associated with mica, leading to different states of such two leaflets.

3.1 Preparation of supported lipid bilayers

Supported lipid bilayers (SLBs) were at the starting point prepared by utilizing fusion of small unilamellar vesicles (SUVs). In the aim to reproduce relevant results that previously have been obtained, the preparation was executed in accordance with [8], which is a preparation method that is highly consistent with the method reported by other references [16][17]. However, satisfying results were only obtained from fusing multilamellar vesicles (MLVs) - that is, by deviating from the methods described by the references.

The lipids used for experiments throughout this project are 1,2-dipalmitoyl-sn-glycero-3-phosphatidylcholine (DPPC) and 1,2-dilauroyl-sn-glycero-3-phosphocholine (DLPC). The lipids were purchased in powder

form from Avanti. To ease the sample preparation prospectively, stock solutions were prepared for each type of lipid by dissolving the respective lipids in a 1:1 methanol:dichloromethane solvent to a concentration of 10mM. The purpose of the solvent is to obtain a solution of evenly distributed separate lipids. The stock solutions were stored at -25°C while sealed with parafilm.

The lipid solutions used to form the SLBs were prepared by mixing the stock solutions to the desired ratio in a vial. To remove the solvent from the lipids, the vial was put under a nitrogen air stream for at least six hours for evaporation, and then in a vacuum pump for at least 4 hours for desiccation. The dry lipids were dissolved in a volume of millipore water to obtain the desired concentration. The concentration of the samples used in the experiments were between 0.5 mM and 3.0 mM.

To obtain MLVs the sample was heated above the melting transition of the lipids in a water bath and then repeatedly vortexed and reheated. This resulted in a milky solution. When SUVs were desired the sample would hereafter be sonicated with a Branson Sonifier model Cell Disruptor B15 in a pulsed mode until it appeared clear. The sample was kept above the melting transition of the lipids before fusing.

From the final solution of vesicles a volume between 50 μL and 100 μL was pipetted onto the mica support which were attached to the bottom of a petri dish. The support used throughout this project was mica. The mica was purchased in plates containing several layers. A layer was cleaved from the plate using double adhesion tape. The freshly cleaved mica was then attached to the bottom of a petri dish with a combination of the double adhesion tape used for cleaving and regular tape.

After pipetting the sample was left to fuse for at least 1 hour. Hereafter the surface of the fused sample was rinsed from unfused vesicles by letting millipore water run over it. Then the sample was covered with a layer of about 0.5 cm of millipore water, and was then ready for scanning.

3.2 Topographic measurements with atomic force microscopy

Atomic force microscopy (AFM) generates three dimensional images based on the interaction between a tip and the surface of the concerned sample (the tip-sample interactions) while the tip is scanned across the surface line by line. The horizontal plane (the xy-plane) is controlled by the parameters set for the resolution of the image. Changes in the vertical direction (the z-direction) are controlled by a feedback mechanism that depends on the interaction between tip and sample.

3.2.1 The ground principle

The effective interaction force that is sensed by the tip during an approach of the sample surface is a sum of different attractive and repulsive forces, and can be approximated as seen in Figure 4. When approaching, the forces will at first be increasingly attractive (negative) until a minimum is reached. The electrostatic forces (the Van der Waal forces) are dominating in this regime and the force depends on the tip-sample distance as $1/r^6$. The turn point at the minimum occurs because Pauli repulsion starts to dominate. The minimum is also the point where the tip gets in touch with the sample surface [22]. The Pauli repulsion occurs due to the Pauli exclusion principle that states that two identical fermions cannot occupy the same quantum state simultaneously [18]. This leads to a withdrawal of the electrons from the interacting side of the atoms. Thus the nuclei of the atom will be exposed leading to a strong repulsion between the nuclei and the force exponentially approaching infinity. The strong dependence on the tip-sample distance makes the method very sensitive in the vertical direction.

Due to the strong distance dependence of the tip-sample force, it is possible to measure the interaction between only the atoms on the apex of the tip and the sample by mounting a sufficiently pointy tip on a bendable cantilever. The forces are measured by utilizing that within the regime of elastic deformation of a spring with spring constant c_z in the z-direction, the extension or compression Δz of the spring is a direct measure of the exerted force $F_{interatomic}$ by

$$F_{interatomic} = c_z \times \Delta z. \quad (3)$$

This is known as Hooke's law [10]. Hence, by mounting the tip on a bendable cantilever, height changes of a surface can be measured by detecting the deflection of the cantilever (assumed that the tip-sample interaction is the same for both the high and the low area).

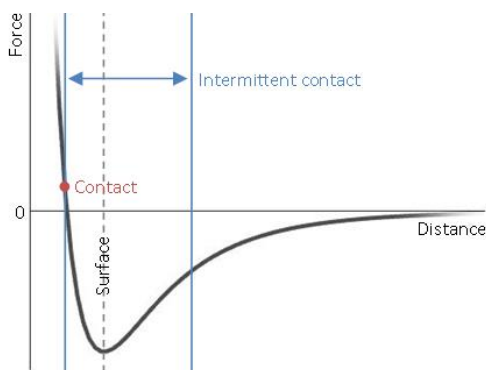


Figure 4: Schematic approximation of the effective interaction force sensed by the tip during an approach of the sample surface. The minimum indicates the position of the sample surface. The tip-sample force for two operating methods, contact mode and intermittent contact mode, are marked on the plot.

3.2.2 Instrumental setup for atomic force microscopy

An overview of the AFM setup is seen in Figure 5. The sample (1) is placed in a petri dish filled with water (2). The petri dish is placed in a heating mechanism used to control the temperature of the sample (not shown). The tip is mounted on a cantilever that is mounted on a support chip. The combined unit is referred to as an *AFM probe* (3). The support chip of the probe is attached to a glass block¹ (9). For large adjustments the height position (z-position) of this glass block is controlled by stepper motors, and for small adjustments it is controlled by a piezoelectric crystal (7). The scanning of the tip over the sample is controlled by applying voltage over a piezoelectric crystal that controls the movement in the xy-plane (8). A sequential scan is generated by correct synchronization of applied voltages, hence the scanning is made line by line. A setpoint is determined before scanning. This setpoint determines the desired tip-sample interaction and is aimed to be kept constant during the scan.

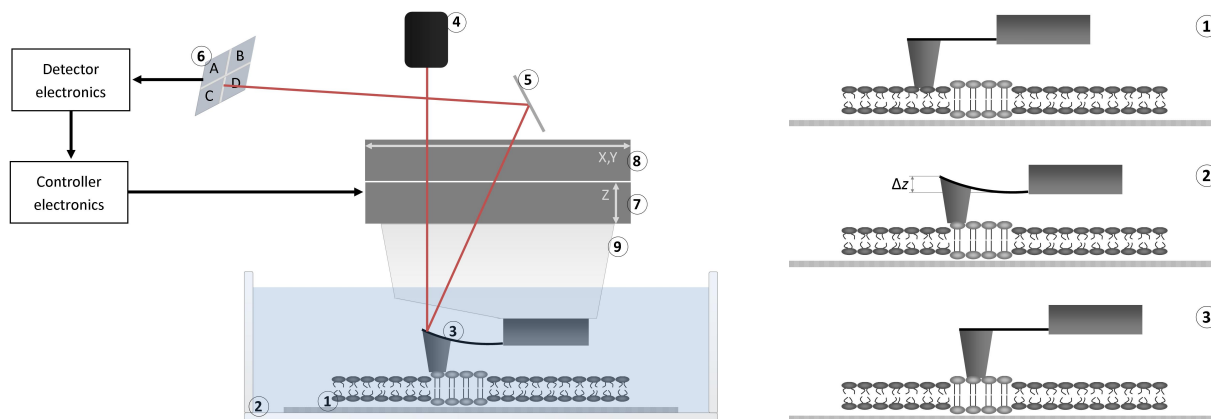


Figure 5: Left: Schematic illustration of a typical AFM setup. A lipid bilayer on a hydrophilic support (1) is placed in a petri dish filled with water (2). A laser beam (4) is deflected on the back of a cantilever with a pointed tip mounted on it (3). The deflected beam hits a mirror (5) that aims it for a sectioned photo-diode (6). The signal from the photo-diode is processed in the detector electronics and sent to the controller electronics that adjusts the height of the support chip by changing the voltage across a piezoelectric crystal (7). The movement in the horizontal plane (the xy-plane) is controlled by a separate piezoelectric crystal (8). The probe is mounted on a glass block (9) that establishes a well-defined interface of the water.

Right: A tip is scanned across an uneven surface with a defined setpoint. As the height of the surface increases, the tip and sample become closer and therefore the tip-sample force is increased. This leads to deflection Δz of the cantilever. To restore the desired tip-sample force the height of the support chip is adjusted by the controller electronics.

¹The glass block is needed if the scanning is performed in liquid, to establish a well-defined interface of the liquid. Without the glass block, waves on the liquid surface would effect the deflection of the laser beam.

As the tip is scanned across an uneven surface it will meet changes in height. Because of the distance dependence for the tip-sample force, this results in bending of the cantilever. The bending of the cantilever is detected by laser beam deflection. A laser beam (4) is targeted at the back of the cantilever, where it is deflected towards a mirror (5) that aims the beam for a sectioned photo-diode (6). Before the sample has been approached, the laser beam is aligned to obtain an equal signal for each of the four sections of the photo-diode. Hence, when the bending of the cantilever deviates from the setpoint value, the beam will hit higher or lower on the photo-diode². This signal is processed in a feedback control loop, where the detector electronics continuously processes the deviation from the desired setpoint. The deviation is minimized by the controller electronics by applying voltage across the piezoelectric crystal that controls the z-direction to adjust the height of the support chip and re-obtain the desired cantilever-bending. The topography images are constructed from these height adjustments.

Different operating modes have been developed for obtaining topographies with AFM. The results for this project has been obtained using *contact mode* since this mode (compared to *intermittent contact mode*³) was found to give the best results. The operating force of both modes are marked on Figure 4. In contact mode the force between the tip and the sample is desired to be kept constant while the tip never leaves the surface. The setpoint value determines the desired deflection of the cantilever. A lower value of the setpoint gives a lower force between the tip and the sample. The setpoint can be converted to the specific tip-sample force if the instrument is calibrated with the cantilever. This was not done in this project.

3.2.3 Important parameters

Spring constant and thermal noise: In order not to damage the sample and to obtain atom resolution the spring constant c_z of a cantilever used in contact mode should be much smaller than the spring constant holding the atoms together on the surface of the sample. The bonding force constant in a crystalline lattice is typically on the order of 1 Nm^{-1} [23]. There is, however, a fundamental limitation for lowering c_z due to oscillations caused by thermal energy. By considering the cantilever as a system with only one degree of freedom (it can only move in the vertical direction), the thermal energy of the system must equal $\frac{1}{2}k_B T$, k_B being Boltzmann's constant and T being the absolute temperature of the system. The thermal energy must equal the elastic energy stored in the cantilever given by $\frac{1}{2}c_z \Delta z$. Hence, the oscillation of the cantilever caused by the thermal energy of the system can be isolated

$$\frac{1}{2}c_z \Delta z^2 = \frac{1}{2}k_B T \Rightarrow \Delta z = \sqrt{\frac{k_B T}{c_z}}. \quad (4)$$

For a cantilever with a spring constant of 0.08 Nm^{-1} this gives oscillations of $\sim 0.24 \text{ nm}$ at temperatures between 25°C and 60°C (the temperatures relevant for this project).

Vertical sensitivity: It can be shown that the change in the position of the deflected laser beam on the photo-diode D due to vertical cantilever deflection is given by

$$D = \frac{3S}{2l} \Delta z, \quad (5)$$

where S is the distance between the point where the laser beam is deflected on the cantilever and the position of the photo-diode, and l is the length of the cantilever. Typical tip-sample forces are on the order of nN. By using equation 3 this causes the deflection of a cantilever with a spring constant of 0.08 Nm^{-1} by the tip-sample forces to be $\sim 10 \text{ nm}$. For a cantilever with $l = 200 \mu\text{m}$ and a laser-beam traveling 5 cm to hit the photo-diode, this gives an amplification of the signal of 375. Since the resolution of a photo-diode is typically $\sim 1 \text{ nm}$, this results in a sub nm precision for the height measurements [22][23].

Influence of scan media: By scanning in liquid the lipid bilayer is not only kept under more stable and natural conditions, the media wherein the sample is scanned also influences the measurement due

²Laser, mirror, photo-diode, glass block and support chip never moves relative to each other.

³In intermittent contact mode the cantilever is forced to oscillate at or near its resonant frequency. During the project the mode was not implemented successfully with cantilevers that were soft enough for scanning lipid bilayers.

to several properties. In air the capillary forces play a central role in the tip-sample interaction. In liquid the electrostatic interactions are the most relevant ones. Thus the media influences the tip-sample forces [23]. Scanning in a liquid generally decreases the tip-sample forces and thereby decreases the damage caused to the sample. But due to a larger change in the angle of the laser-beam caused by the refraction at a water-glass interface compared to at an air-glass interface, the media can also increase the sensitivity of the measurements (see Appendix A.1).

Artifacts related to the geometry of the tip: The finite dimensions of apex of the tip of the AFM probe causes higher features to appear larger than reality, and lower features to appear smaller than reality because the tip cannot get to the corners. This is particularly relevant when scanning features with dimensions that are smaller than the tip dimensions.

3.3 Processing of raw data

The motion of the probe is either perfectly parallel with the surface [23], nor is the motion of the probe perfectly linear in the z-direction [14]. Hence the scanned surface will often appear to be bowed or tilted in the raw data. Since these structures are generally larger than the features of interest, it is necessary to subtract a background from the topography in order to enhance the features of interest. The procedure is called *leveling*. For the topography images shown in this project firstly a planar polynomial of suitable degree has been subtracted from the whole image, and then a polynomial fit of suitable degree, based on values between a lower and upper limit, was subtracted from each line independently. The leveling was done using JPK Data Processing by JPK Instruments. After leveling the data was exported as ASCII files and further processing was performed in MatLab.

3.4 List of materials

Chemicals and lipids:

- 1,2-dipalmitoyl-sn-glycero-3-phosphatidylcholine (DPPC) purchased from Avanti. The lipids have two hydrocarbon chains with length 16:0 (i.e the chains are saturated with only single bonds), and a transition temperature at 41°C.
- 1,2-dilauroyl-sn-glycero-3-phosphocholine (DLPC) purchased from Avanti. The lipids have two hydrocarbon chains with length 12:0 (i.e the chains are saturated with only single bonds), and a transition temperature at -2°C.
- The solvent is mixed from Methanol purchased from VWR and Dichloromethane purchased from EMSURE

Equipment:

- The atomic force microscope used is a NanoWizard II from JPK Instruments mounted on an optical microscope from Olympus model IX71 and connected to a PetriDishHeater from JPK Instruments. The microscopes are installed on a vibration isolation system from Table Stable model IX71 to minimize mechanical oscillation. The setup is placed in a Faraday cage to minimize electronic noise.
- The type of probe used for obtaining the main part of the results in this project is the model PNP-TR purchased from Nano World. The probe has two triangular cantilevers - a harder and a softer one. The triangular shape minimizes the lateral bending of the cantilever. The softer cantilever was used, i.e. a cantilever with a spring constant of $\sim 0.08 \text{ Nm}^{-1}$ and a tip with a typical radius below 10 nm. The data sheet and images of the probe is seen in Appendix A.2.
- For one series of results (see Section 3.5.4) an ACTA probe purchased from AppNano was used. The probe has one rectangular cantilever with a spring constant of $\sim 40 \text{ Nm}^{-1}$ and a tip with a radius guaranteed below 10 nm. The data sheet and images of the probe is seen in Appendix A.3.

- Calibration Grid 32400 was purchased from NanoScience Instruments. Produced in silicon and has a structure consisting of a $2\ \mu\text{m}$ square pattern with a $4\ \mu\text{m}$ period. The square mesas has heights in the range of 25 nm.
- For sonication a Branson Sonifier model Cell Disruptor B15 was used.

3.5 Results

AFM topographies of temperature induced phase transitions were successfully obtained for a mica-supported DPPC bilayer in water. This was not possible until several technical issues had been ruled out though, and it was only the results from the last scans of a supported lipid bilayer, where the vesicles that were used for fusion, in contrary to the methods used in [8][24][16][17][20], was not sonicated.

The topographies are represented as two-dimensional plots, where the two axis represents the horizontal plane. The vertical direction is represented by a color scale. Brighter colors represent higher areas, and darker colors represent lower areas. The color scale of each topography image has been modified to visually enhance the features in the image by adjusting the boundaries of the color map used for plotting.

3.5.1 First results

For the first many results the topographies repeatedly turned out to be inconsistent with the results reported in the literature [8][24][16][17][21][20]. For pure DPPC step heights of ~ 3.0 nm were observed at 25°C (see Figure 6, left). No domains should appear at this state, therefore only step heights due to defects in the bilayer were expected, i.e. step heights of between ~ 5.0 nm and ~ 6.0 nm. Also for two component bilayers of 65:35 DPPC:DLPC step heights of ~ 3.0 nm were observed at 25°C (see Figure 6, center), making the features of the one and two component membranes indistinguishable. Step heights of ~ 1 nm were expected. Several times the mica surface was found to be covered in only very small dots (see Figure 6, right).

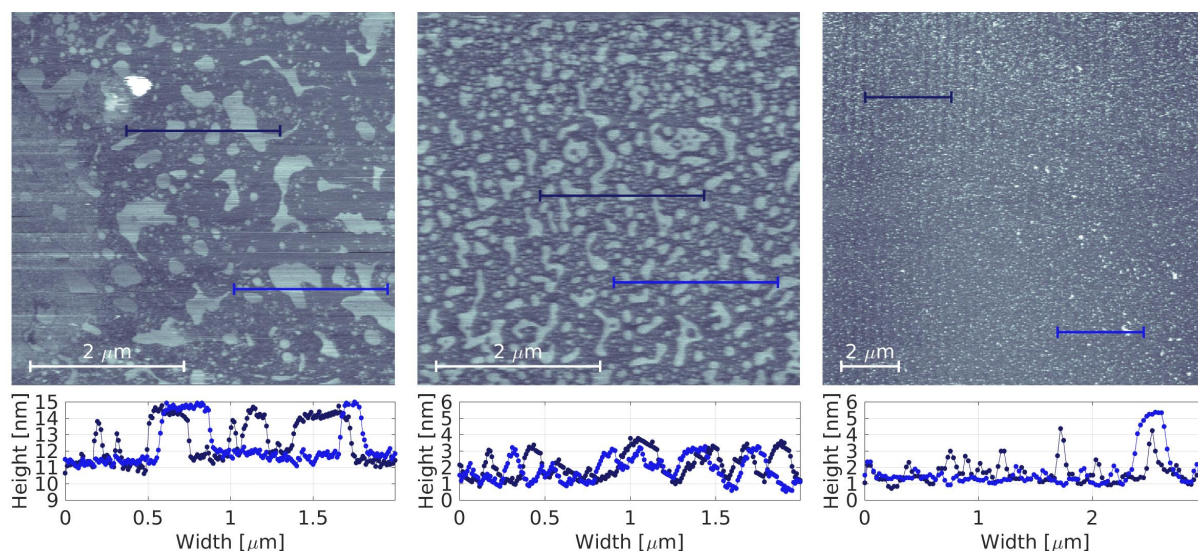


Figure 6: AFM topography images showing scans of what should be supported lipid bilayers in water. The colored lines in the images indicate the position of the height profiles. Left: 3 mM DPPC. Center: 2 mM 65:35 DPPC:DLPC. Right: 1 mM DPPC.

The results were considered to be an indication of a problem with the fusion of vesicles on the mica surface or a contaminated stock solutions. Therefore both the fusion method was reconsidered and a new DPPC stock solution was prepared. This did not result in more convincing results though.

3.5.2 Scanning of mica

Clean mica surfaces were scanned to ensure the flatness of the surface and to exclude that the structure of the mica surface was contributing to the features seen in the scans of supported lipid bilayers. A representative example is seen in Figure 7. The results show that the structure of the mica surface is very clean and easy to distinguish from a bilayer since only height steps between ~ 0.2 nm and ~ 0.3 nm are observed (cf. Section 3.2.3 i.e. in the range of the estimated oscillations due to thermal energy for the cantilever that was used). These heights appears to be much less extended in the horizontal plane than any feature caused by lipids. The melting transition of mica is between 700°C and 1000°C . Hence, no phase transition will be observed within the temperature interval relevant for this project.

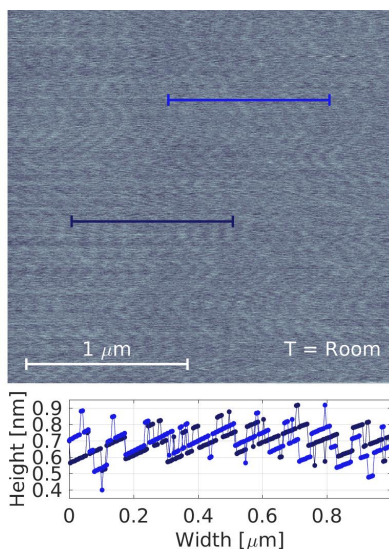


Figure 7: AFM topography image showing a scanning of freshly cleaved mica in water at room temperature. Height variations between ~ 0.2 nm and ~ 0.3 nm are observed.

3.5.3 The influence of media and setpoint on scannings of a calibration grid

A calibration grid of silicon claimed to have step heights of ~ 25 nm was scanned both in air (see Figure 8, left) and in water (see Figure 8, right) with different setpoints. The full scan series obtained in air is seen in Appendix A.4. In air the scans were performed with setpoints increasing from 0.1 V to 1.0 V. In water the scans were performed first with the setpoint increased from 0.1 V to 1.2 V and then with the setpoint decreased from 1.2 V to 0.1 V. On the day where the scans were performed in water the calibration grid appeared contaminated despite repeated rinsing of both the calibration grid and the probe. For each of the scans both in air and water the difference between three squares in the calibration grid and the lower area was calculated. This was done by selecting an area on the top of the squares of the calibration grid and a counter area in the lower part of the calibration grid⁴. These areas are marked by dashed squares in Figure 8. Each set of counter area has its own color. For each area the absolute height is calculated individually for each vertical line by averaging the points in that line. Height differences were calculated for each of the vertical lines by subtracting the averaged values. Then the calculated height differences for each set of counter areas were averaged to obtain the final value for the height difference for that set of counter areas. The result of this procedure is seen in Figure 9. A clear inconsistency of the measured heights is observed.

⁴Due to the leveling procedure, where a polynomial line fit is subtracted from each vertical line, the horizontal lines become incomparable. This is seen quite pronounced in the height profiles for Figure 8, right, where the lines are shifted in height. Therefore all height measurements must be obtained in the vertical direction.

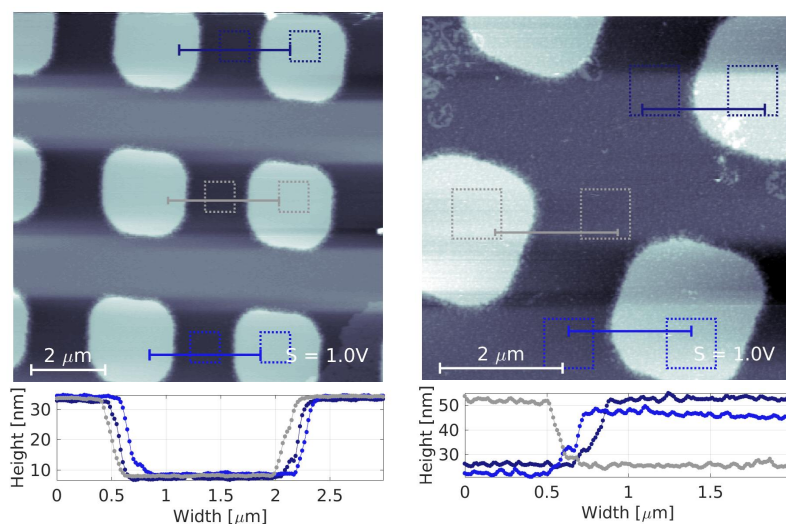


Figure 8: AFM topography images showing scans of a calibration grid claimed to have height steps of ~ 25 nm and appertaining height profiles. The colored lines in the images indicate the position of the height profiles. The dashed squares indicate the areas where from the height steps in Figure 9 has been calculated. Left: Scanning obtained in air with a setpoint of 1.0 V. Right: Scanning obtained in water with a setpoint of 1.0 V.

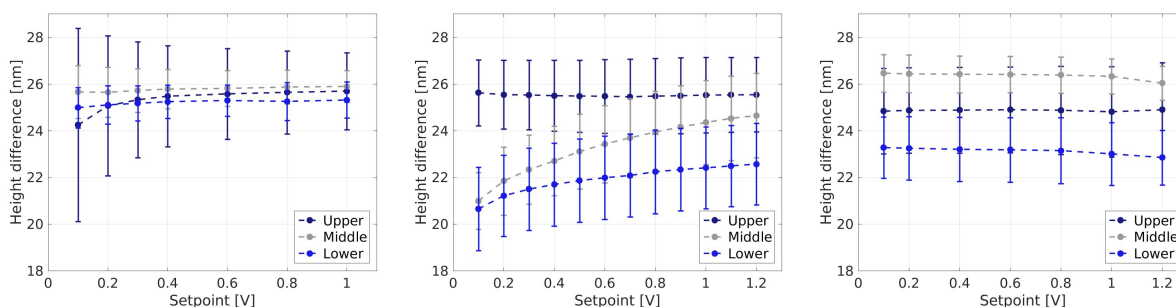


Figure 9: Calculated height steps from an AFM topography of a calibration grid claimed to have height steps of ~ 25 nm. The calculations are made from the areas marked by dashed squares in Figure 8. Left: Calculated from scans obtained in **air** while **increasing** the setpoint for each scanning. Center: Calculated from scans obtained in **water** while **increasing** the setpoint for each scanning. Right: Calculated from scans obtained in **water** while **decreasing** the setpoint for each scanning.

When the scans were obtained with increasing setpoint two of the calculated heights appeared to be strongly influenced by the change in setpoint. But the influence was not reversed when the setpoint was decreased again, suggesting that the change might occur over time and not due to changing setpoint.

It must be noted that despite setting the AFM to repeat scanning the same area, a small drift in the position for each scanning occurs. Therefore the selected areas do not correspond exactly to each other for each scanning. The drift can be seen in Appendix A.4.

3.5.4 The effect of cantilever spring constant on SLBs

To explore the effect of a spring constant that exceeds the bonding force constant between the lipids on the surface of a sample ($\sim 1 \text{ Nm}^{-1}$), a sample of (attempted) lipid bilayers were scanned using a probe with a cantilever with a spring constant of $\sim 40 \text{ Nm}^{-1}$. The result is seen in Figure 10. For these scans (and only these scans) the ACTA probe was used. First, several scans were performed for a smaller area. For the first scan (Figure 10, left) lipid features are observed on the surface. Afterwards this area appeared bare for several scans. By increasing the area of the scan it was clear that the lipids in the smaller area had been scratched of the surface (Figure 10, right).

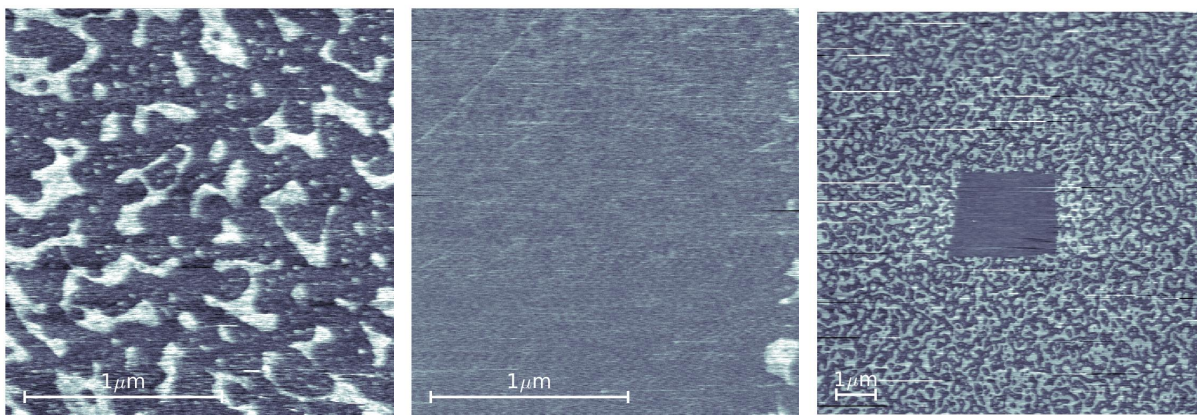


Figure 10: AFM topography images showing how a cantilever, with a spring constant that exceeds the bonding constant on the surface of the sample, effects a DPPC sample.

3.5.5 The effect of setpoint on SLBs

To explore the effect of the setpoint on lipid bilayers a bilayer⁵ was scanned several times in the same area with a setpoint of 0.1 V. An example from these scans is seen in Figure 11, left. Then the scan was repeated with a setpoint of 0.5 V and then of 1.0 V. The results are seen in Figure 11, center and right, respectively. It is seen that minimal damage is caused to the bilayer for a setpoint of 0.1 V, while much damage is caused to the bilayer already at a setpoint of 0.5 V. The damage is seen as the holes in the bilayer.

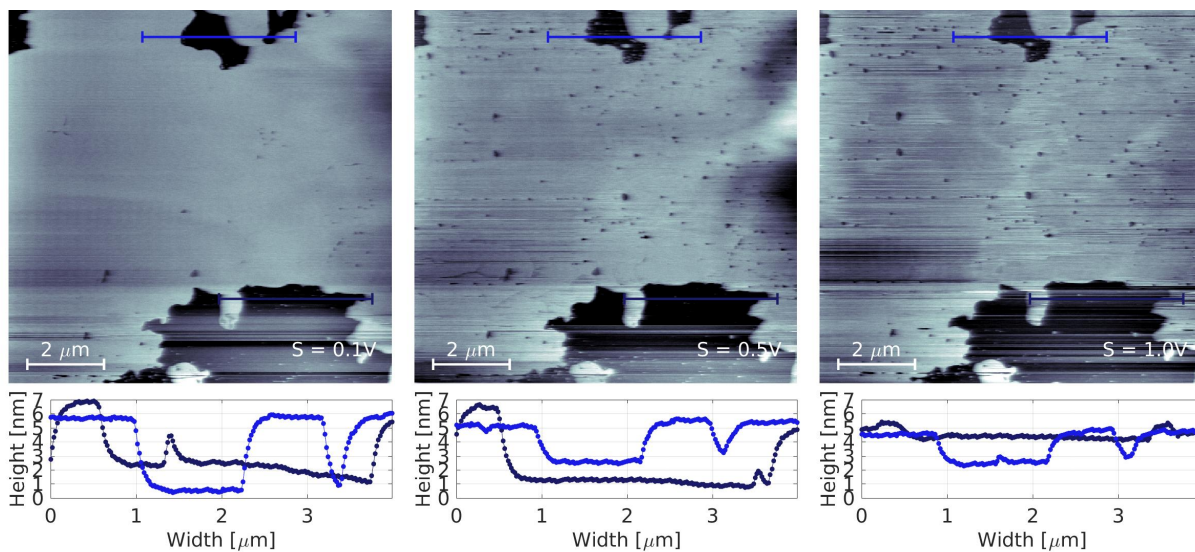


Figure 11: AFM topography images showing scans of a 1 mM DPPC bilayer with increasing setpoint. Left: Obtained with a setpoint of 0.1 V. Center: Obtained with a setpoint of 0.5 V. Right: Obtained with a setpoint of 1.0 V.

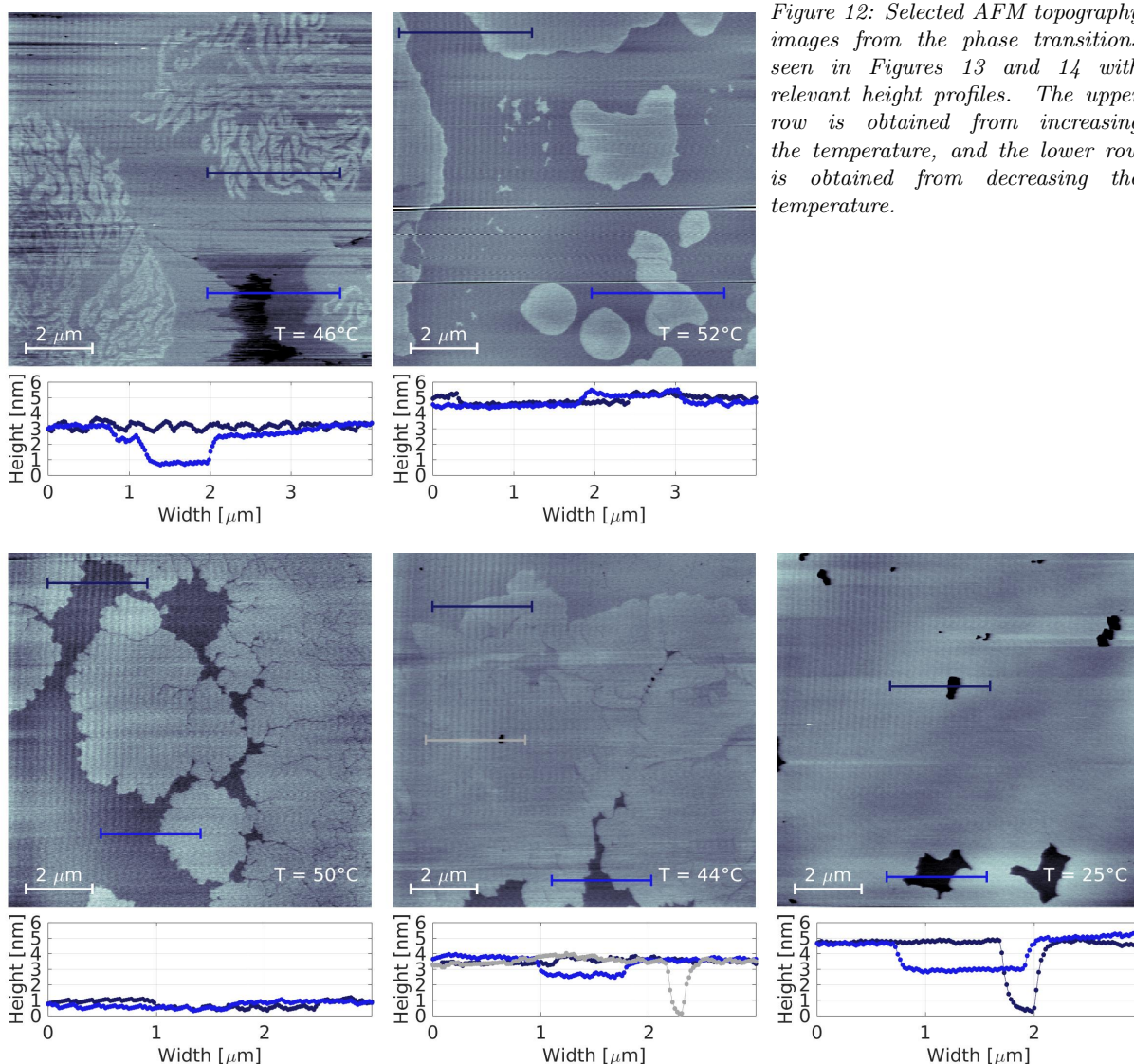
For each topography height profiles are obtained for the same coordinates. For the topography obtained with a setpoint of 0.1 V both height profiles show step heights of ~ 5.0 nm. In the topography obtained with a setpoint of 0.5 V the brighter blue height profile appear to be only ~ 2.5 nm while the darker blue height profile is consistent with the previous. For the topography obtained with a setpoint of 1.0 V the brighter blue height profile appear to be only ~ 2.0 nm while the darker blue height profile shows almost no height variation. Hence, also for lipid bilayers inconsistency in the height measurements

⁵The first and only successfully obtained bilayer.

are observed. The inconsistency appeared to be increased when the setpoint was increased, and seemed to be caused by lipids that were dragged from the bilayer structure. This is anticipated both from the increase in lines in the fast scan direction and from the increase in chunks that shows up in the areas assumed to be bare mica. It appears that a higher setpoint both leads to contamination of the tip and damaging of the bilayer structure.

3.5.6 Temperature induced phase transition in DPPC SLB

For the sample also discussed in Section 3.5.5, phase transitions were induced by first increasing the temperature (see Figure 13) and afterwards decreasing the temperature (see Figure 14). It was not possible to scan the same area throughout the transitions due to problems with approaching the sample. The scans are all obtained with a setpoint of 1.4 V or higher, as this turned out to be experimentally necessary in order to obtain any measurements.



By increasing the temperature above the melting point of a DPPC bilayer supported by mica, formation of lower domains was observed. This indicated a gel-fluid transition. Because these features were growing independent of the fast scan direction it was found reasonable to classify them as features of the phase transition and not as artifacts. Two transitions were observed within the temperatures between

40°C and 58°C. One transition between 40°C and 50°C (referred to as the first up-transition), and one transition between 52°C and 54°C (referred to as the second up-transition). In the first up-transition the lower domains were growing in lines, whereas in the second transition the lower domains were to a higher degree surrounding the higher domains, indicating that different interactions were dominating for the two transitions.

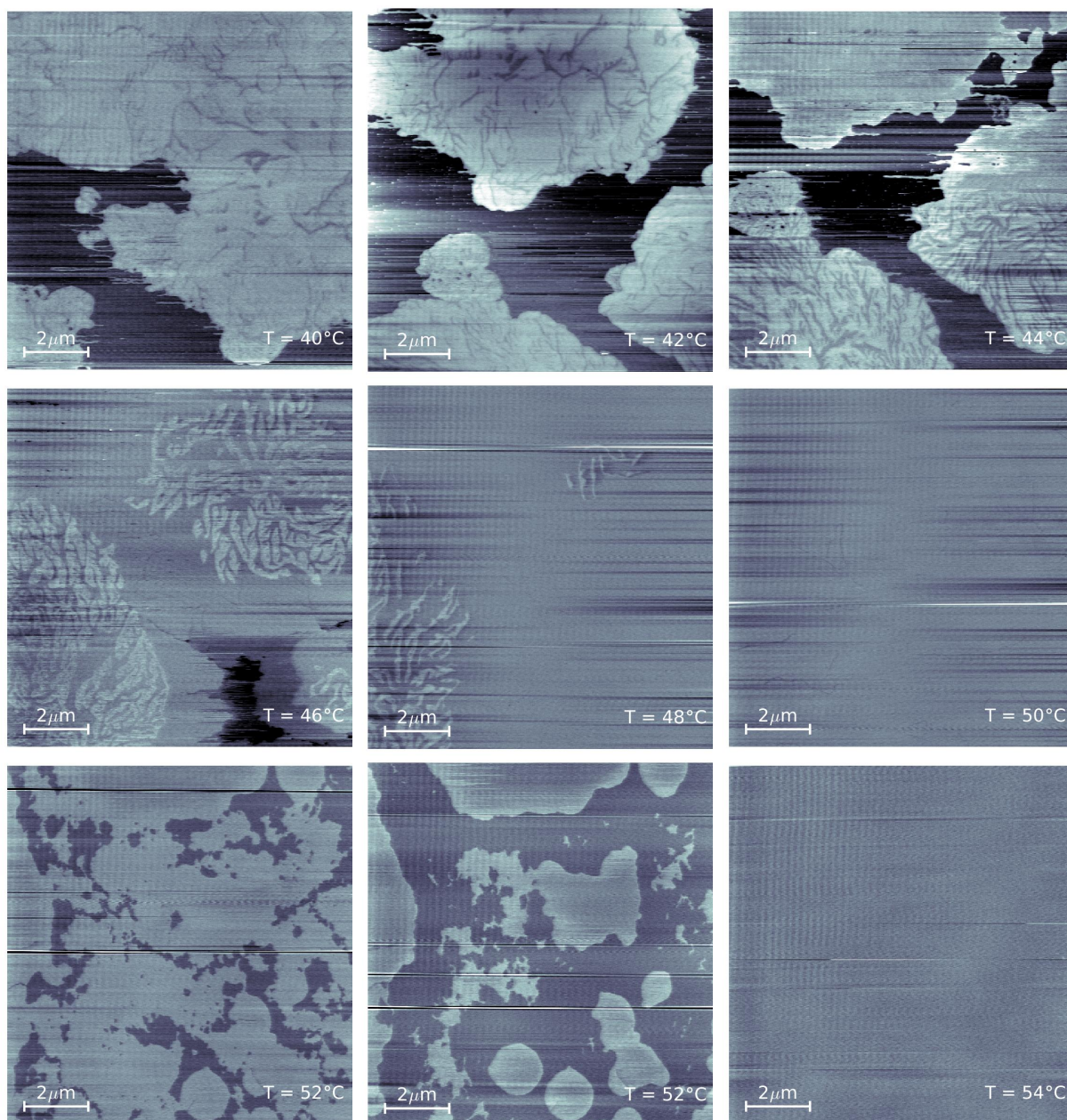


Figure 13: AFM topography images showing phase transition in a DPPC bilayer in water at increasing temperature. Two transitions are observed: The first up-transition between 40°C and 50°C, and the second up-transition between 52°C and 54°C.

When decreasing the temperature afterwards, formation of higher domains were observed. This indicated a fluid-gel transition. One transition was observed within the temperatures between 58°C and 40°C (referred to as the down-transition). In this transition the higher domains were growing in rounded shapes with rugged perimeters, indicating a third type of domain where again different interactions were

dominating.

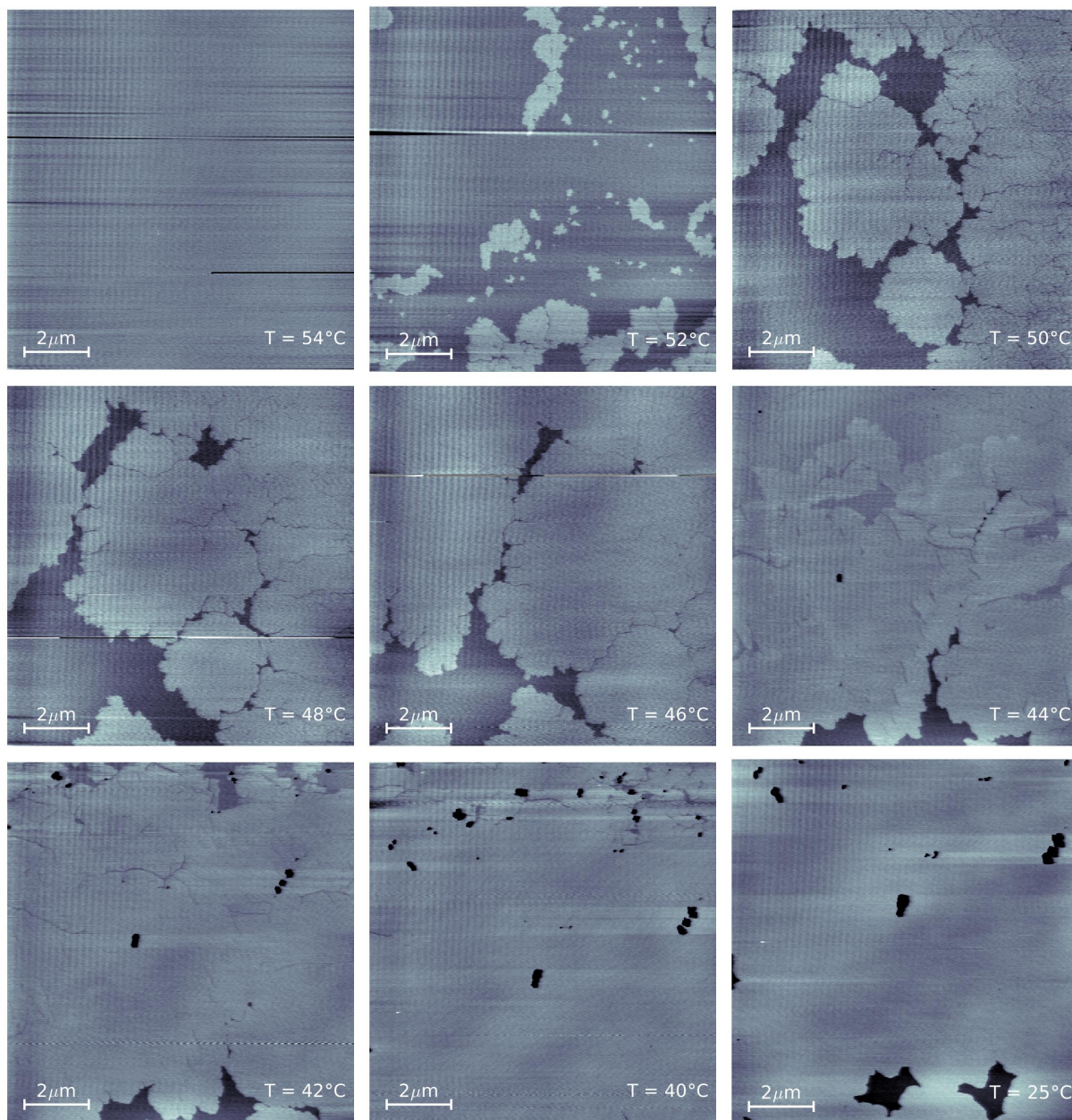


Figure 14: AFM topography images showing the phase transition in a DPPC bilayer in water at decreasing temperature. One transition is observed between 52°C and 40°C.

Height profiles has been obtained for AFM topographies containing all types of the observed domains. The selected AFM topographies are seen in Figure 12. The upper row is obtained from the up-transition, and the lower row is obtained from the down-transition.

For the top-left image, obtained at 46°C during the first up-transition, the darker blue height profile marks a line containing both a higher and a lower domain. Height steps of between ~ 0.5 nm and ~ 0.8 nm are observed. The brighter blue height profile marks a line showing a defect in the bilayer structure (i.e. a discontinuation). It is seen that it is a defect from the lines caused by lipids that have been dragged along by the tip due to the high setpoint. The bottom of the hole appears to be ~ 2.5 nm lower than the highest lipids. At the edge of the whole an area of lipids that are ~ 1.0 nm lower than the main part of

melted lipids is observed.

For the top-center image, obtained at 52°C during the second up-transition, both the darker blue height profile and the brighter blue height profile marks lines containing lower domains of lipids that have and have not went through the second transition. Height steps of ~ 0.6 nm are observed.

For the bottom-left image, obtained at 50°C during the down-transition, both the darker blue height profile and the brighter blue height profile marks lines containing domains of lipids that have and have not went through the transition. Height steps of ~ 0.5 nm are observed.

For the bottom-center image, obtained at 44°C also during the down-transition, the gray height profile marks a line containing a defect in the bilayer. The bottom of the hole appears to be ~ 3.5 nm lower than the surrounding bilayer. The darker blue height profile marks a line that contains an area of some higher and lower lipids. Height steps of ~ 0.5 nm are observed. The brighter blue height profile marks a line that appears to contain an area of some higher and lower lipids. Height steps of ~ 1.5 nm are observed.

For the bottom-right image, obtained at 25°C at decreasing temperature, the darker blue line extends across what appears to be a defect in the bilayer. Height steps of ~ 4.8 nm are observed. The brighter blue line extends across what appears to be another defect. Height steps of ~ 2.0 nm are observed.

4 Discussion and conclusions

The aim of this project was to utilize atomic force microscopy to study domain formation during temperature induced phase transitions in supported lipid bilayers, based on the associated height changes. After ruling out several technical issues and determining some experimental limitations, results were obtained for a DPPC bilayer. It was found that the phase transition observed for increasing temperature occurred in two steps, while the phase transition observed for decreasing temperature occurred in one step. Different domain formation was observed for each of the transitions.

4.1 Disclosure of experimental limitations

Inconsistent height measurements were observed both within and between AFM topographies obtained for a calibration grid. Since the bonding forces in silicon are much higher than the tip-sample force, the tip could not be perturbing the surface. Thus, it was found unreasonable to make any quantitative analysis of height steps. For lipid bilayers it appeared that a higher setpoint lead both to damaging of the bilayer structure and contamination of the tip, and thereby contributed to the incorrect height detections by compromising the tip-sample interactions. This result indicated that the setpoint should be kept as low as possible when scanning lipid bilayers. However, this was not possible when inducing phase transitions as it was found instrumentally necessary to increase the setpoint considerably in order to even approach the sample.

4.2 Temperature induced phase transitions in a mica-supported DPPC bilayer

For the scans of temperature induced phase transitions in mica-supported DPPC bilayers the up-transition was found to be split into two, while the down-transition was found to occur as one. Similar results has been obtained by Leonenko et al. [17], where splitting of the phase transition were observed for both the up- and down-scan though. Also the temperature intervals for the transitions differ compared to the findings in this project. This is a parameter easily influenced by the rate of temperature change though.

Also from measurements with differential scanning calorimetry (DSC) the mica-support has been shown to cause splitting of the phase transition for DPPC bilayers. This was done by Yang and Appleyard [25] (see Figure 15, left), where mica supported bilayers were prepared by coating microscopic chips of mica with DPPC by vesicle fusion. Their results show three peaks in the temperature interval between 41°C and 46°C. It is suggested that the two peaks at the highest temperatures corresponds to separate transitions in the higher and lower leaflet of the bilayer associated with the mica-support, respectively, and that the peak at the lowest temperature corresponds to the transition of the top bilayer of the double bilayer as well as residual lamellar vesicles in the suspension. These results differ from the results

obtained, when DSC measurements are obtained for lamellar DPPC bilayers (see Figure 15, right), and emphasizes that the mica-support influences the phase transition of lipid bilayers when associated with such. It is suggested by Yang and Appleyard that both the broadening and the splitting of the phase transition could be caused by a coupling between the lower leaflet and the mica support, that causes the two leaflets of the bilayer to have separate main phase transitions. Coupling between the two leaflets has earlier been conjectured to be weak [25]. Hence, if the coupling between the lower leaflet and the mica support is stronger, the symmetry for the leaflets will break. But it is emphasized that the existence of a main phase transition in supported bilayers indicate that they do behave as normal bilayers, and thus are relevant as models for biological membranes.

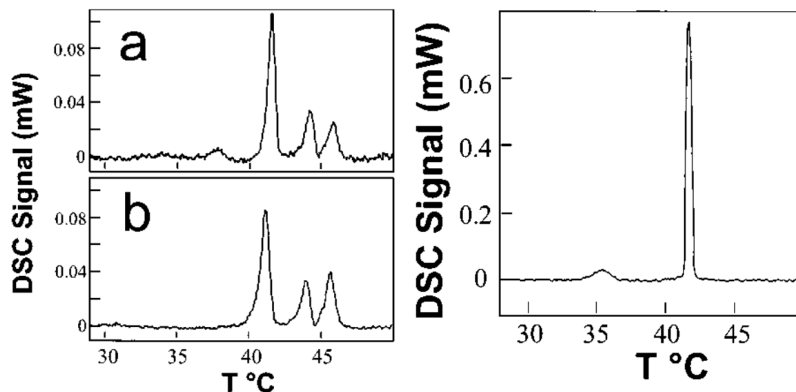


Figure 15: Results obtained by Yang and Appleyard [25] from differential scanning calorimetry. Left: Results for supported DPPC bilayers where (a) is for an initial DSC scan and (b) is for an average of six subsequent DSC scans. Right: Results for lamellar DPPC bilayers.

A more narrow phase transition is observed for the DSC results by [25] compared to the results obtained from AFM. This could, cf. cooperativity, of the lipids indicate that the bilayer peaces from where the AFM topographies are obtained in general consists of fewer lipids than the vesicles used for the DSC measurements.

The findings by Yang and Appleyard suggests that the first up-transition observed in this project would correspond to the melting of the lower leaflet of the single bilayer that is associated with the mica, and the second up-transition would correspond to the melting of the higher leaflet in the single bilayer. The very distinct difference in the domain formation for the first and second up-transition indicates that some coupling between the two leaflets do occur.

Thickness changes has been experimentally determined for squid axons during the propagation of nerve signals [5]. The height changes associated with the transitions of the DPPC bilayer could be a similar phenomenon. This would correspond to an increase in the membrane capacitance, which contradicts the Hodgkin-Huxley model for propagation of nerve signals, where the membrane capacitance is assumed to be constant. The membrane capacitance C_m is given by

$$C_m = \epsilon_0 \epsilon \frac{A}{D}, \quad (6)$$

where ϵ_0 is the permittivity for air, ϵ is the permittivity of the dielectric medium between the leaflets, A is the surface area, and D is the distance across the membrane. The change in area of the head groups of DPPC has been found to change with 24% during the main phase transition. In this project the distance across the membrane was found to change with $\sim 17\%$. This would result in a change in the capacity in the range of 65%, indicating a non-negligible change in the membrane capacitance during the propagation of a nerve signal.

4.3 Further explorations

The experiments should be repeated several times to ensure reproducibility. After further improvement of the method, the aim is to extend the study of domain formation to multi component bilayers in temperature induced phase transitions, and to study the effect of anesthesia on the domain formation. It

is known that as a consequence of ideal mixing of the anesthetic drugs in the fluid phase of the membrane and exclusion from the solid phase, general anesthetics decrease the main phase transition of biological membranes [26]. Such experiments could bring insight to the influence of anesthesia on the membrane organization.

5 References

- [1] S. Singer et al., *The Fluid Mosaic Model of the Structure of Cell Membranes*, Science (1972), 175:4023:720-731
- [2] O. Mouritsen et al., *Mattress Model of Lipid-Protein Interactions in Membranes*, Biophys. J. (1984), 46:141-153
- [3] W. Osdol et al., *Measuring the kinetics of membrane phase transitions*, J. Biochem. Biophys. Methods (1989), 20(1):1-46
- [4] A. Hodgkin et al., *A Quantitative Description of Membrane Current and its Application to Conduction and Excitation in Nerves*, J. Physiol. (1952), 117:500-544
- [5] T. Heimburg et al., *On soliton propagation in biomembranes and nerves*, PNAS (2005), 102:9790
- [6] T. Heimburg, *Die Physik von Nerven*, Physik Journal 8 (2009), 3
- [7] T. Heimburg, *Thermal Biophysics of Membranes*, WILEY-VCH, 2007
- [8] V. Oliynyk, *Experimental study of lipid membranes: lipid domain formation and peptide aggregation (2005)*, PhD thesis, Georg-August-Universität zu Göttingen
- [9] J. Dreier, *Orientalional Texture of Lipid Bilayer and Monolayer Domains* (2012), PhD thesis, University of Southern Denmark
- [10] H. Young et al., *University Physics* 13th edition (2013), Addison-Wesley
- [11] O. Mouritsen et al., *Life - As a Matter of Fat* (2005), Springer
- [12] G. Binnig et al., *Atomic Force Microscope*, Physical Review Letters (1986), 56:9
- [13] WC Lin et al., *Lipid Asymmetry in DLPC/DSPC-Supported Lipid Bilayers: A Combined AFM and Fluorescence Microscopy Study*, Biophysical Journal (2006), 90:228-237
- [14] P. West et al., *A Guide to AFM Image Artifacts*, Pacific Nanotechnology
- [15] S. Morandat et al., *Atomic force microscopy of model lipid membranes*, Anal Bioanal Chem (2013), 405:1445-1461
- [16] V. Ivanova, *Analyzing Heat Capacity Profiles of Peptide-Containing Membranes: Cluster Formation of Gramicidin A*, Biophysical Journal (2003), 84:2427-2439
- [17] Z. Leonenko et al., *Investigation of Temperature-Induced Phase Transitions in DOPC and DPPC Phospholipid Bilayers Using Temperature-Controlled Scanning Force Microscopy*, Biophysical Journal (2004), 86:3783-3793
- [18] D. Griffiths, *Introduction to Quantum Mechanics* 3rd edition (2013), Pearson
- [19] N. Kahya et al., *Probing Lipid Mobility of Raft-exhibiting Model Membranes by Fluorescence Correlation Spectroscopy*, The Journal of Biological Chemistry (2003), 278:28109-28115
- [20] S. Landa, *Influence of voltage on phase behavior of membranes* (20013), Master thesis, University of Copenhagen
- [21] JPK application note, *Lipid rafts: Phase separation in lipid bilayers studied with atomic force microscopy*
- [22] G. Schmid et al., *Nanotechnology - Volume 6: Nanoprobes* (2009), WILEY-VCH
- [23] A. Baró et al., *Atomic Force Microscopy in Liquid* (2012), WILEY-VCH
- [24] V. Oliynyk et al., *Defect formation of lytic peptides in lipid membranes and their influence on the thermodynamic properties of the pore environment*, Biochimia et Biophysica Acta (2007), 1768:236-245
- [25] J. Yang et al., *The Main Phase Transition of Mica-Supported Phosphatidylcholine Membranes*, J. Phys. Chem. B (2000), 104:8097-8100
- [26] K. Græsboell et al., *The Thermodynamics of General and Local Anesthesia*, Biophysical Journal (2014), 106:2143-2156

A Appendix

A.1 Increased sensitivity due to refraction index

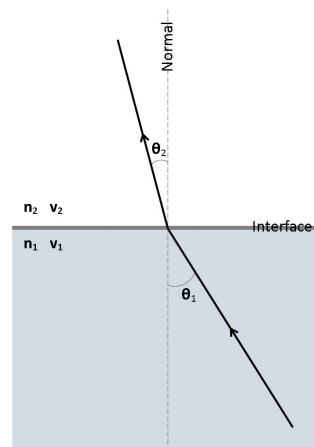
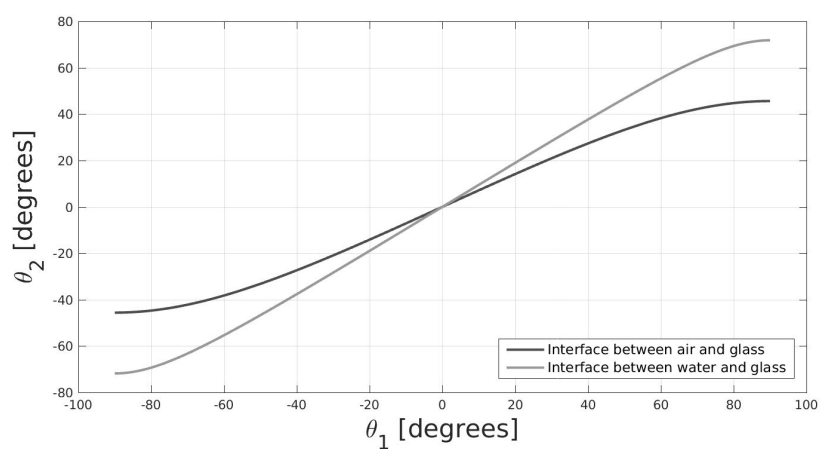


Figure 16: The effect of refraction.

A.2 AFM probe: PNP-TR-20 purchased from NanoWorld

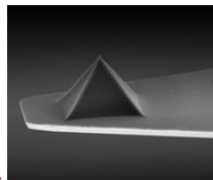


Type: **PNP-TR**

Pyrex-Nitride Probe – TRIangular Cantilevers

Cantilever Data*	Cant. 1	Cant. 2
Shape	Triangular	
Resonance Frequency	67 kHz	17 kHz
Force Constant	0.32 N/m	0.08 N/m
Length	100 µm	200 µm
Mean Width	13.5 µm	28 µm
Thickness	0.5 µm	0.5 µm

*Typical values
Guaranteed values



Pyrex-Nitride oxide sharpened, pyramidal tip

Product Description

Leading edge in sharpness and durability

NanoWorld Pyrex-Nitride probes are designed for various imaging applications in contact or dynamic mode.

The Pyrex-Nitride probes have silicon nitride cantilevers with very low force constants and integrated oxide sharpened, pyramidal tips with a height of 3.5 µm. The tip is located 4 µm behind the free end of the cantilever. The probe series features a support chip that is made of Pyrex. The TR series features two different triangular cantilevers. Both sides of the chip have identical cantilevers.

The typical tip radius of curvature is below 10 nm.

All chips are pre-separated prior to shipment and come in Gel-Pak containers.

[Close](#)

Coating Description

The gold reflex coating deposited on the detector side of the cantilevers enhances the reflectance of the laser beam. As the coating is almost stress-free the bending of the cantilevers due to stress is less than 2 degrees.

Order Codes and Packages Sizes

Order Code	Quantity	Data Sheet
PNP-TR-20	20	yes
PNP-TR-50	50	yes

For more information contact: info@nanoworld.com

Gel-Pak® is a registered trademark of Delphon Industries.
All data are subject to change without notice.

NanoWorld AG
Rue Jaquet-Droz 1
Case Postale 216
CH-2002 Neuchâtel
Switzerland
www.nanoworld.com

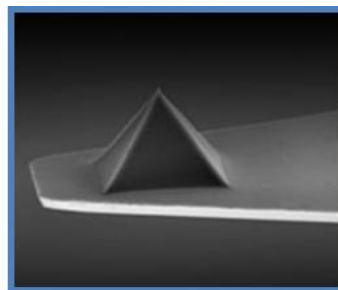
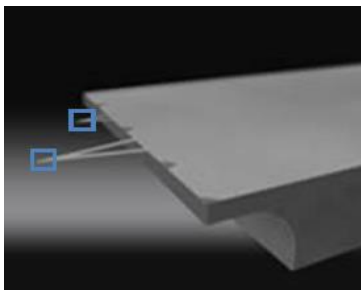


Figure 17: The tip of PNP-TR-20.

A.3 AFM probe: ACTA purchased from AppNano

Technical Specifications Sheet

Probe Model: ACTA

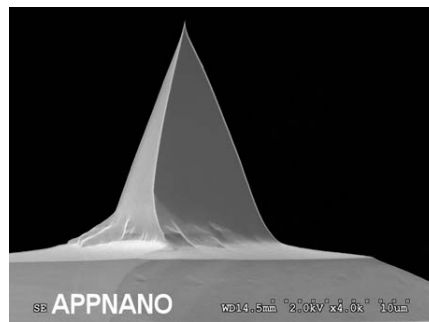
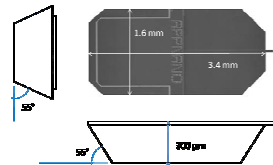
APPNANO probes are compatible with most commercially available SPMs. These probes are nanofabricated using highly doped single crystal silicon with unparalleled reproducibility, robustness and sharpness for consistent high resolution imaging capabilities.

The **ACTA Probe** is designed for Non-Contact / Tapping Mode / Intermittent Contact / Close Contact applications. The ACTA probes have a high frequency that allows faster scanning speeds.

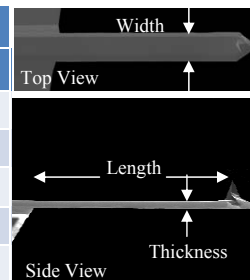
Handle Chip Specifications	
L x W x T	3.4 mm x 1.6 mm x 300 μ m
Alignment Grooves	YES

Tip Specifications	
Shape	Pyramidal
Height (μ m)	14 - 16
ROC (nm)	6
Coating	None

Cantilever Specifications	
Material	Si
Shape	Rectangular
Front Coating	None
Reflex Side Coating	Al, 30 nm \pm 5 nm



Parameter	Value		
	Nominal	Minimum	Maximum
Spring Constant (N/m)	40	25	75
Frequency (kHz)	300	200	400
Length (μ m)	125	115	135
Width (μ m)	35	30	40
Thickness (μ m)	4.5	4.0	5.0



Ordering Information	
Part Number	Probes
ACTA-10	10
ACTA-20	20
ACTA-50	50
ACTA-200	200
ACTA-W	410 - 424

NOTES :

1. The specification range is **guaranteed**. The values of spring constant and frequency are calculated using mathematical formulation.
2. These probes feature **alignment grooves** compatible with all alignment chips available in the market.
3. Please contact our **Distributor** in your area to **order** the probes.
4. For more technical information, please contact either our distributor in your area or e-mail us directly at info@appnano.com.

Applied NanoStructures, Inc.
1700 Wyatt Dr. Suite 12, Santa Clara, CA 95054, USA

Tel: 1 408 567 0115 Fax : 1 408 516 4917

E-mail : info@appnano.com



www.appnano.com

A.4 Drift in position for each scanning

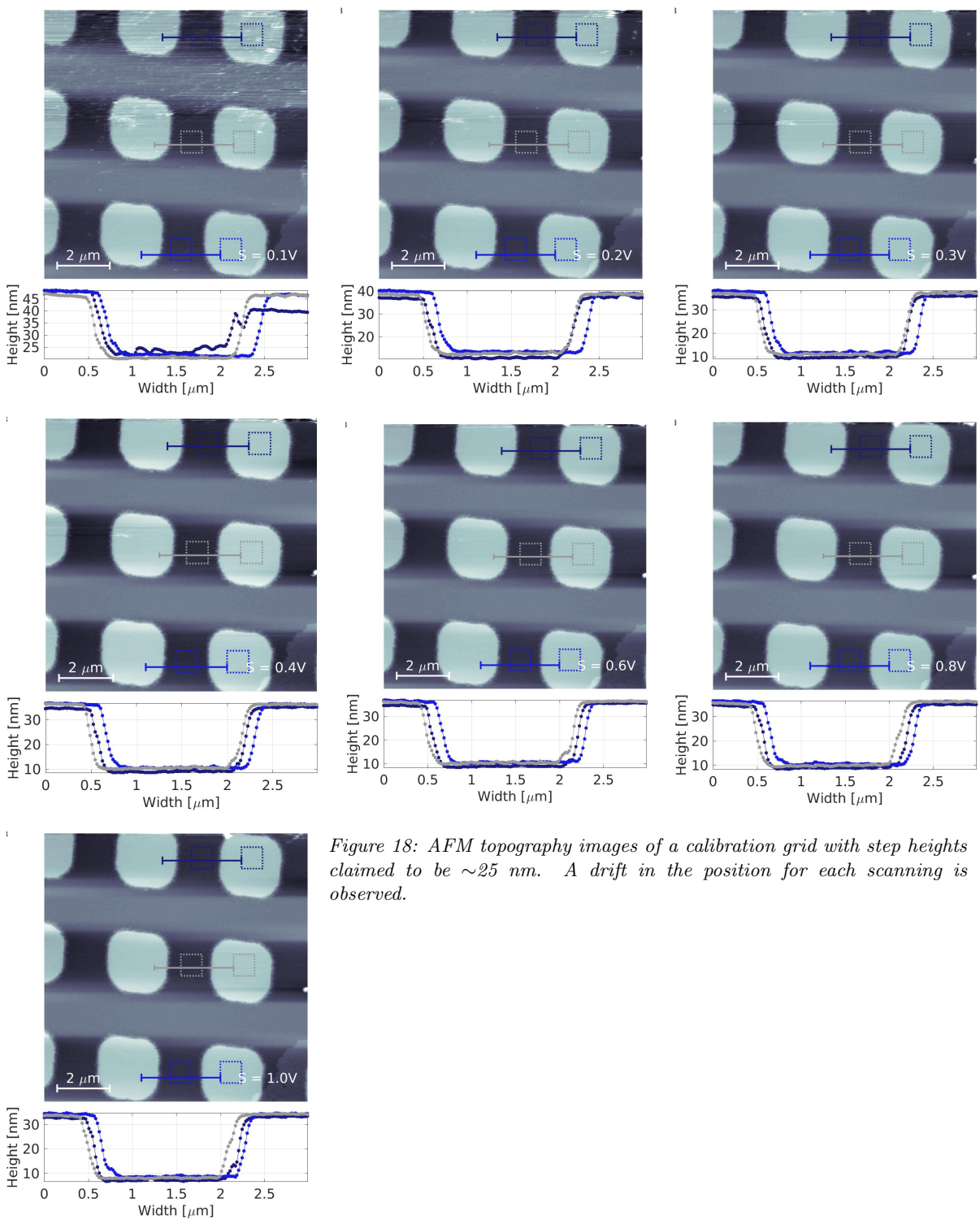


Figure 18: AFM topography images of a calibration grid with step heights claimed to be ~ 25 nm. A drift in the position for each scanning is observed.